Supporting Information

to

Biotin Functionalization of 8-Hydroxyquinoline Anticancer Organometallics: Low *in vivo* Toxicity but Potent *in vitro* Activity

Tasha R. Steel,[1] Julia Stjärnhage,[1] Zexiong Lin,[1] Hugh O. Bloomfield,[1] Caitlin D. Herbert,[2] Jonathan W. Astin,[2] Krzysztof Krawczyk,[3] Błażej Rychlik,[3] Damian Plażuk,[4] Stephen M.F. Jamieson,[5] Christian G. Hartinger[1,*]

[1] School of Chemical Sciences, The University of Auckland, Private Bag 92019, Auckland 1142, New Zealand

[2] Department of Molecular Medicine and Pathology, Faculty of Medical and Health Sciences, University of Auckland, Private Bag 92019, Auckland 1142, New Zealand

[3] Centre for Digital Biology and Biomedical Science – Biobank® Lodz, Faculty of Biology and Environmental Protection, University of Lodz, ul. Pomorska 141/143, 90-236 Łódź, Poland

[4] Laboratory of Molecular Spectroscopy, Department of Organic Chemistry, Faculty of Chemistry, University of Lodz, Tamka 12, 91-403 Łódź, Poland

[5] Auckland Cancer Society Research Centre, University of Auckland, Private Bag 92019, Auckland 1142, New Zealand.

Contents

^{1}H and ^{13}C{^{1}H} DEPT-Q NMR spectra, and ESI-mass spectra for L1 and L2

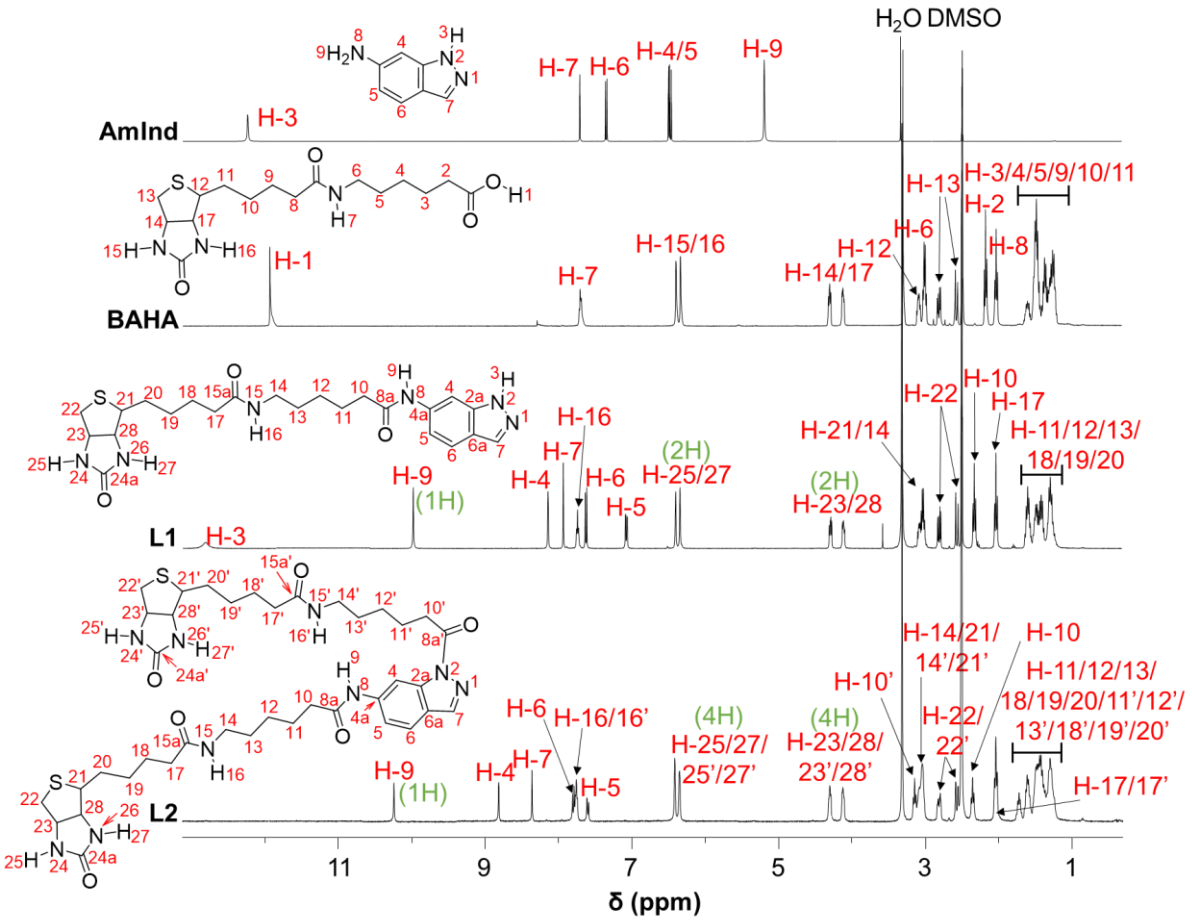

Figure S1. ^{1}H NMR spectrum of ligands **L1** and **L2** with comparison to starting materials 6-aminoindazole (AmInd) and biotinyl-6-aminohexanoic acid (BAHA) in d_6-DMSO.

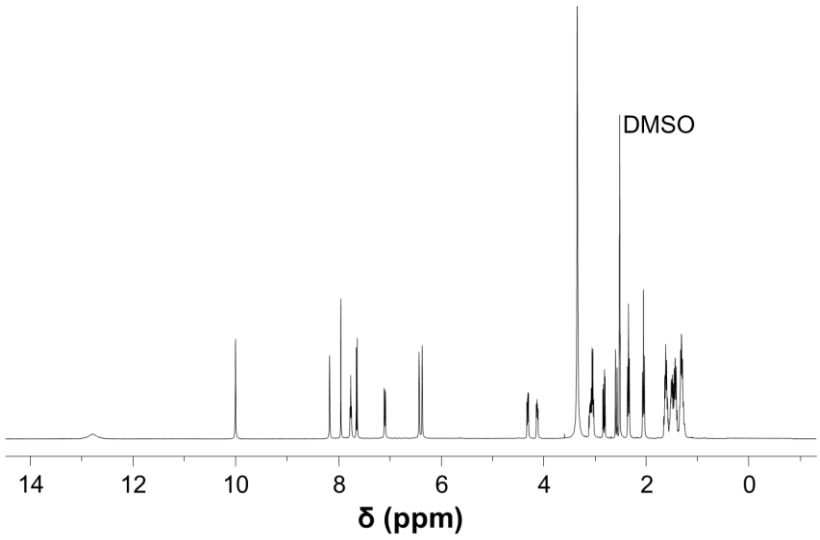

Figure S2. ^{1}H NMR spectrum of **L1** in d_6-DMSO.

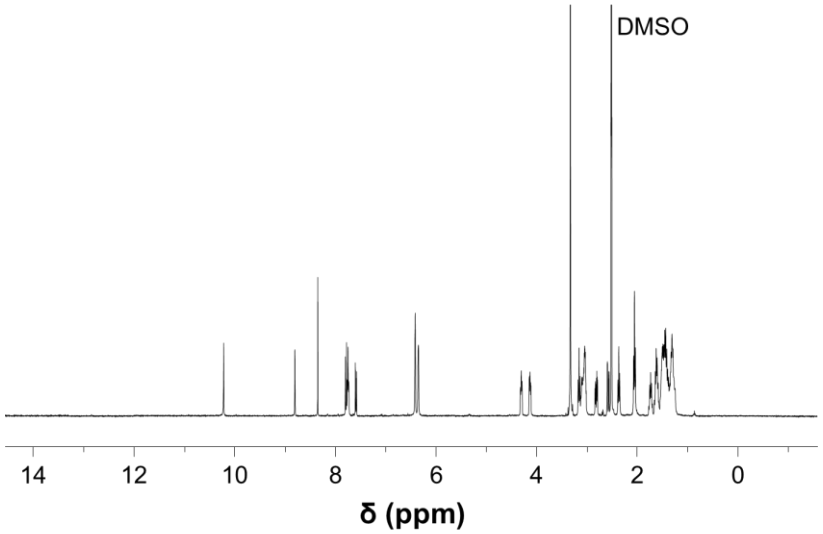

Figure S3. ^{1}H NMR spectrum of **L2** in d_6-DMSO.

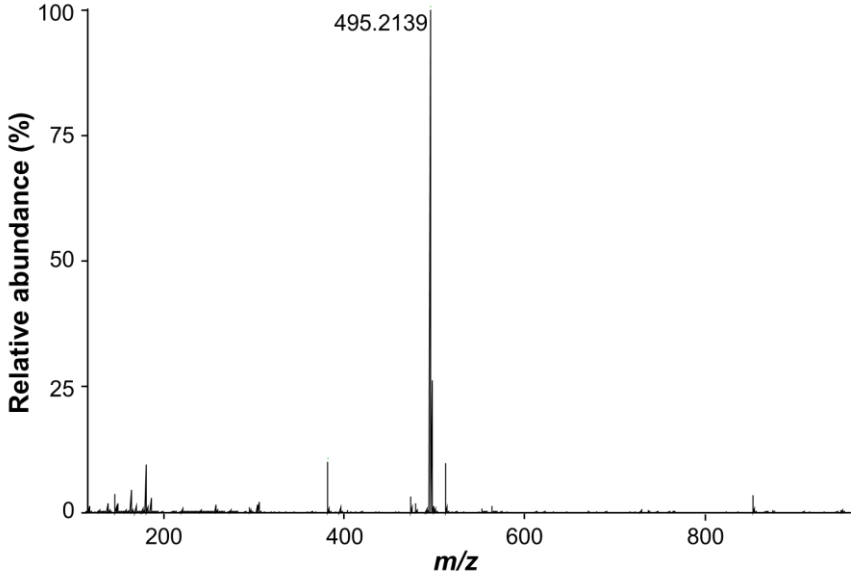

Figure S4. ESI-mass spectrum of **L1** indicating the base peak at *m/z* 495.2139 assigned to [**L1** + Na]$^{+}$.

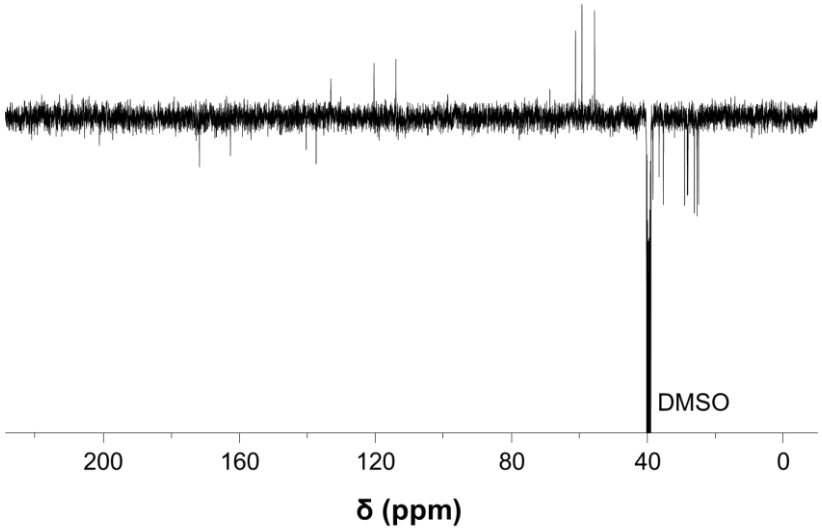

Figure S5. $^{13}C\{^{1}H\}$ DEPT-Q NMR spectrum of **L1** in d_6-DMSO.

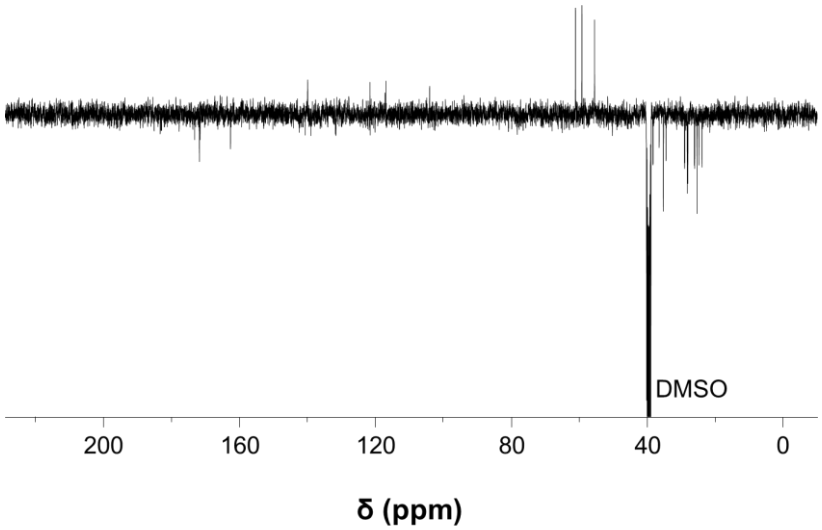

Figure S6. $^{13}C\{^{1}H\}$ DEPT-Q NMR spectrum of **L2** in d_6-DMSO.

^{1}H and ^{13}C{^{1}H} DEPT-Q NMR spectra, and ESI-mass spectra for 1a–1d and 2a

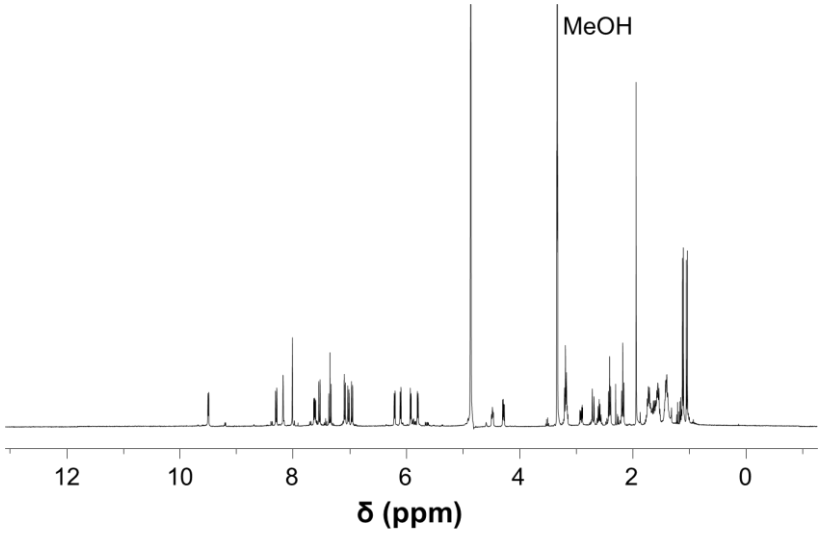

Figure S7. ^{1}H NMR spectrum of **1a** in d_4-methanol.

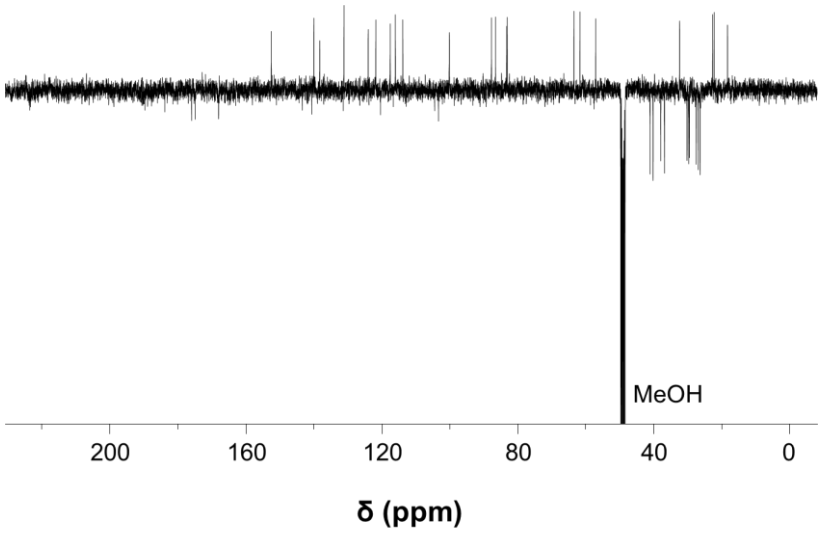

Figure S8. ^{13}C{^{1}H} DEPT-Q NMR spectrum of **1a** in d_4-methanol.

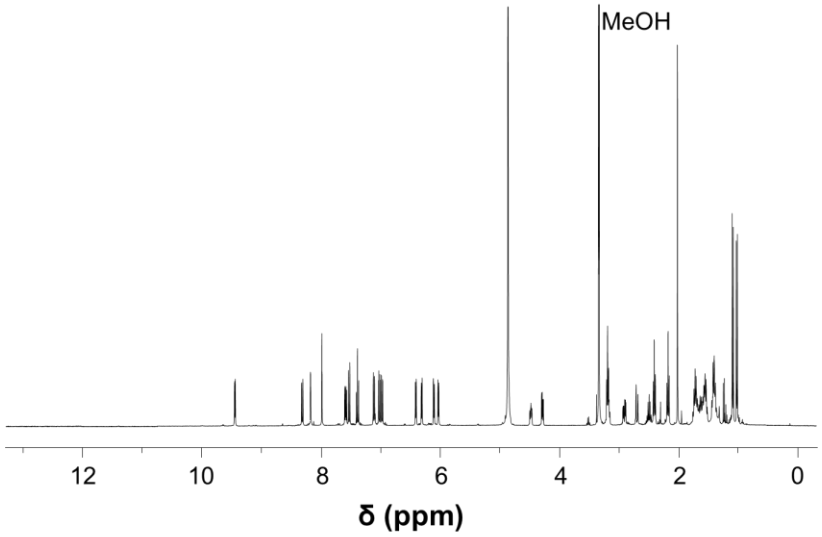

Figure S9. ^{1}H NMR spectrum of **1b** in d_4-methanol.

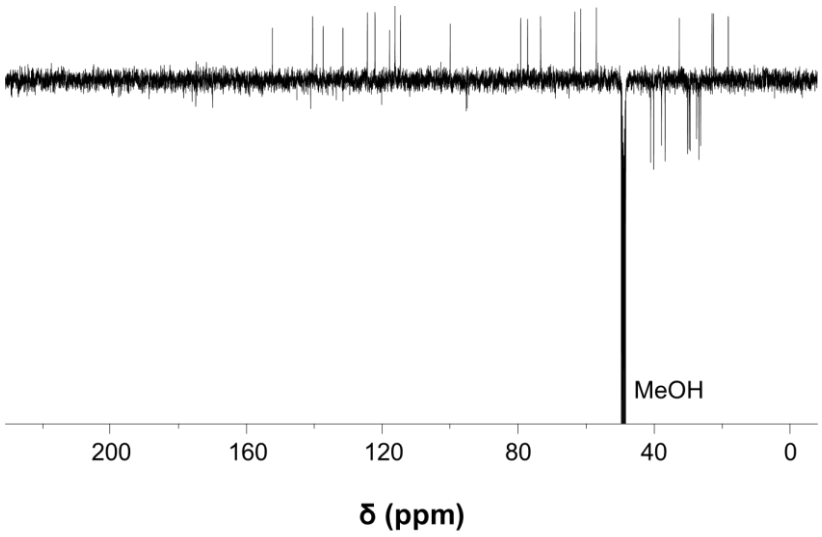

Figure S10. ^{13}C{^{1}H} DEPT-Q NMR spectrum of **1b** in d_4-methanol.

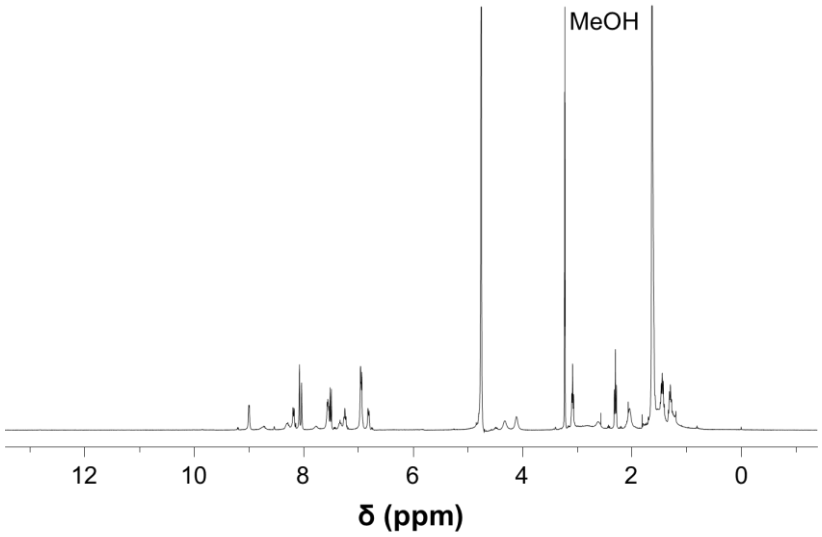

Figure S11. ^{1}H NMR spectrum of **1c** in d_4-methanol.

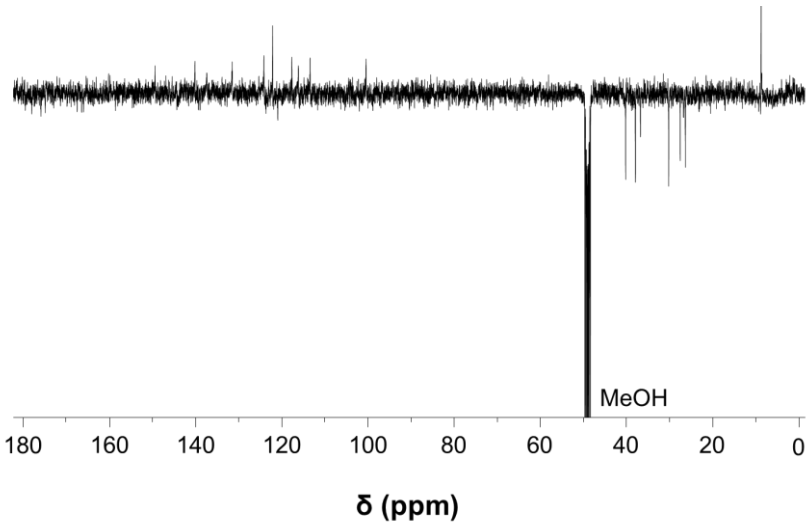

Figure S12. ^{13}C{^{1}H} DEPT-Q NMR spectrum of **1c** in d_4-methanol.

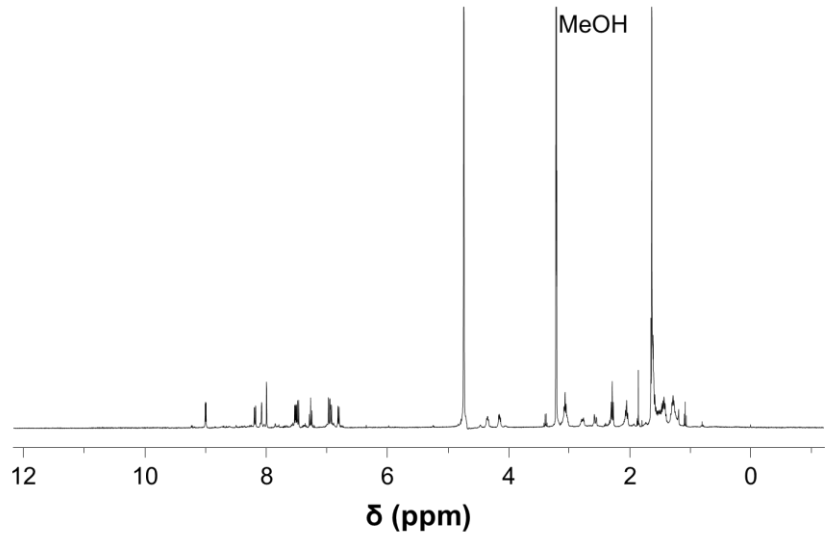

Figure S13. ^{1}H NMR spectrum of **1d** in d_4-methanol.

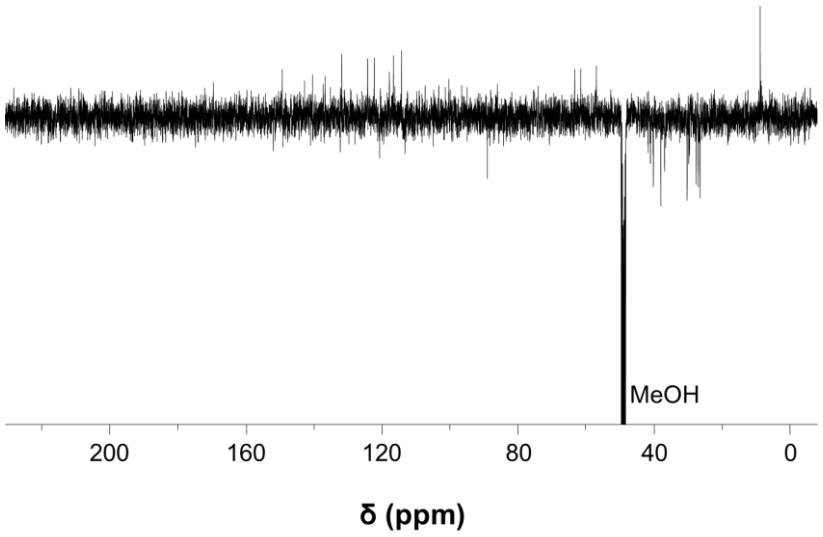

Figure S14. ^{13}C{^{1}H} DEPT-Q NMR spectrum of **1d** in d_4-methanol.

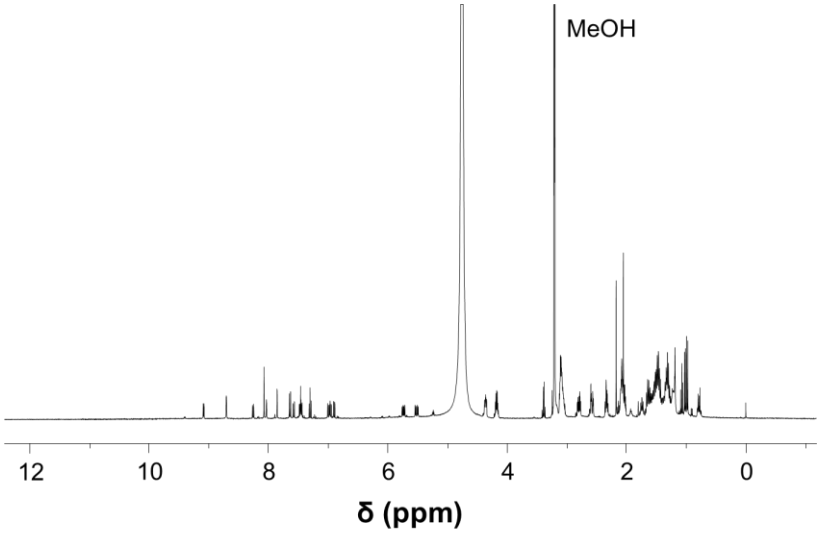

Figure S15. ^{1}H NMR spectrum of **2a** in d_4-methanol.

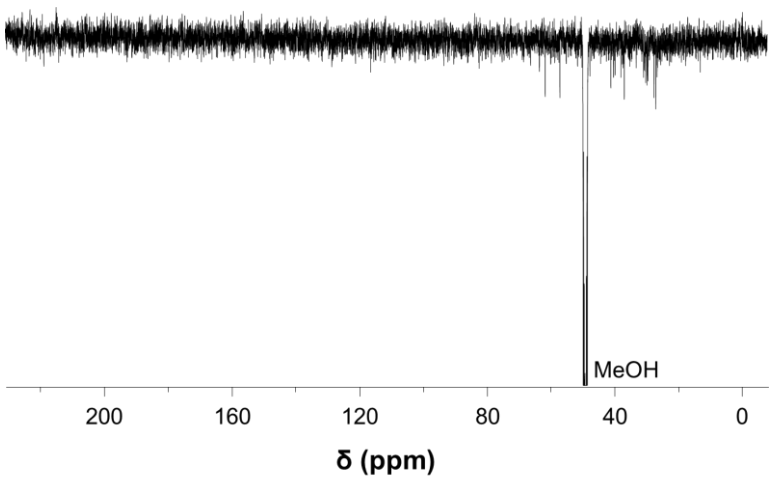

Figure S16. ^{13}C{^{1}H} NMR spectrum of **2a** in d_4-methanol.

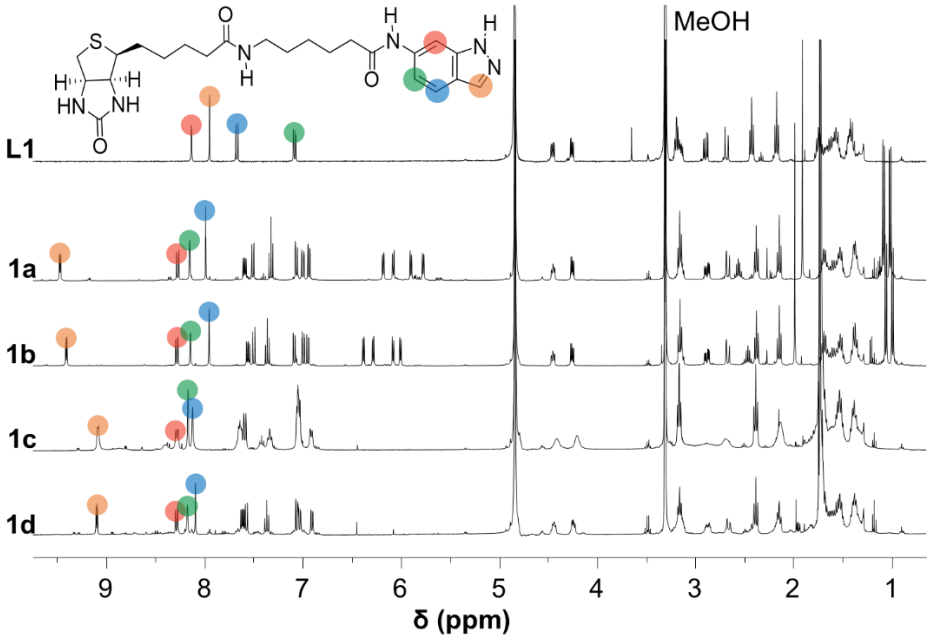

Figure S17. ^{1}H NMR spectrum of ligand **L1** with comparison to complexes **1a**–**1d** in d_4-methanol. The coloured dots indicate the downfield shifting observed upon coordination of **L1** to the metal centres.

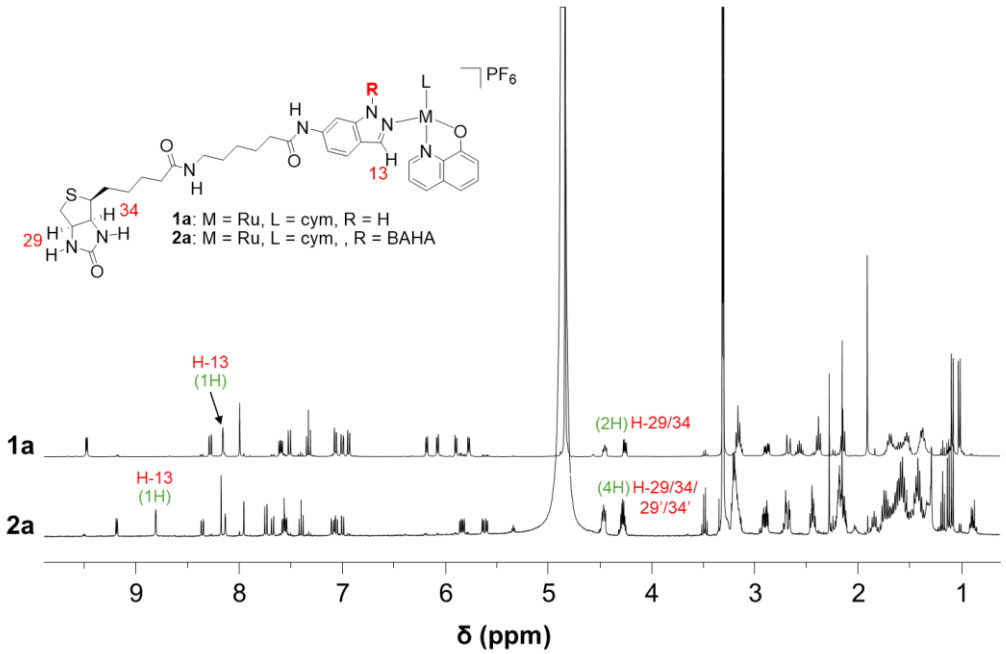

Figure S18. Comparative ^{1}H NMR spectra for Ru complexes containing one (**1a**) or two (**2a**) biotinyl units in d_4-methanol, showing the relative integration values of the aminoindazole and biotinyl groups.

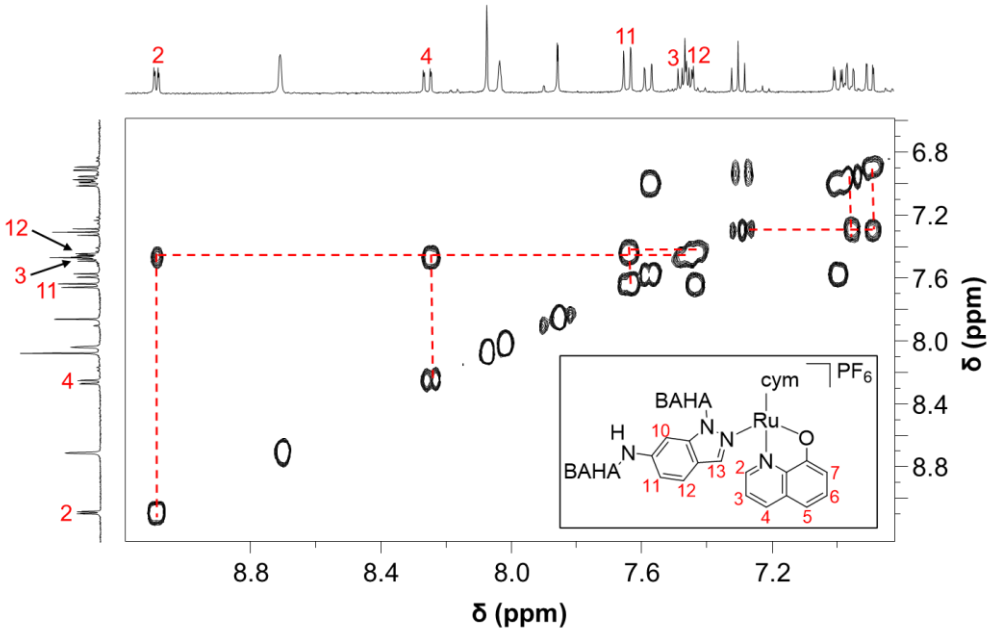

Figure S19. ^{1}H-^{1}H COSY NMR spectrum of Ru complex **2a** in d_4-methanol.

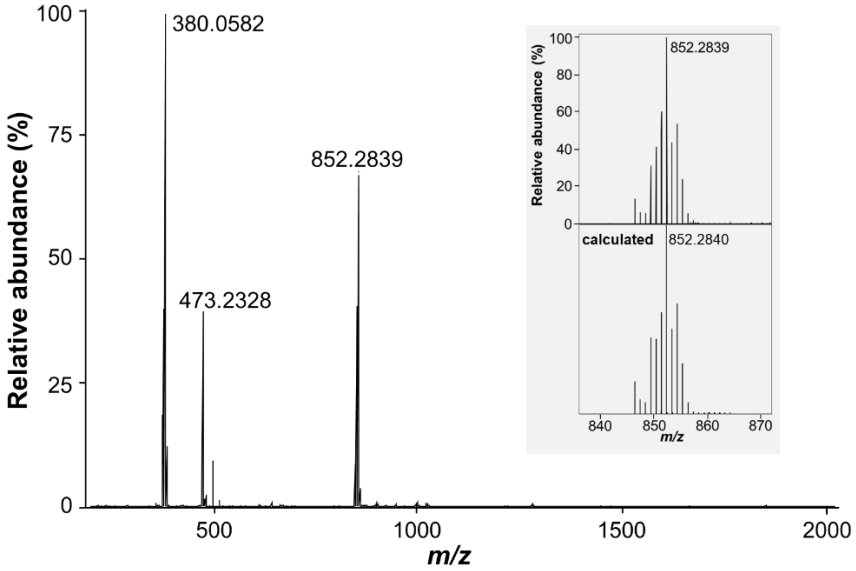

Figure S20. ESI-mass spectrum of **1a**. The inset shows the peak at *m/z* 852.2839 assigned to [**1a** – PF_6]$^+$ (m/z_{calc} 852.2840).

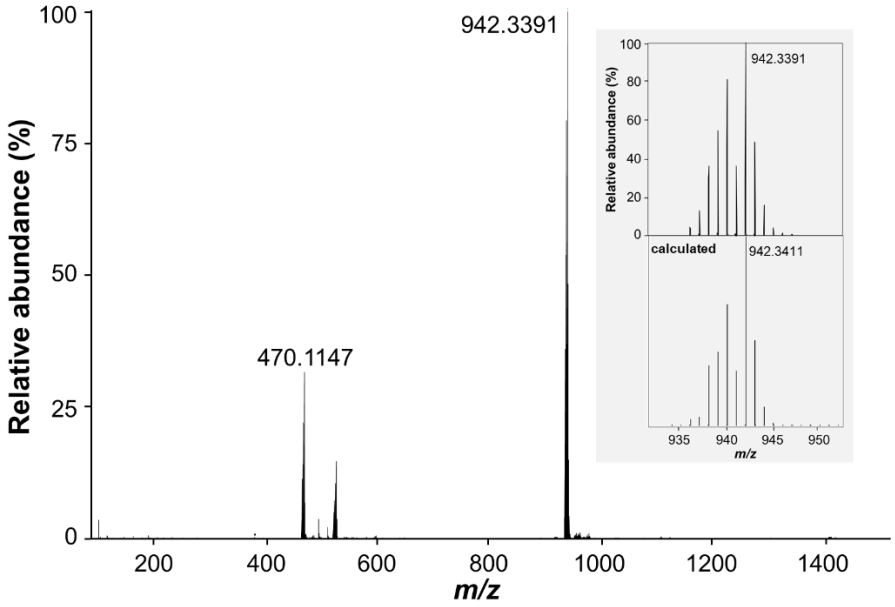

Figure S21. ESI-mass spectrum of **1b**. The inset shows the base peak at *m/z* 942.3391 assigned to [**1b** – PF_6]$^+$ (m/z_{calc} 942.3411).

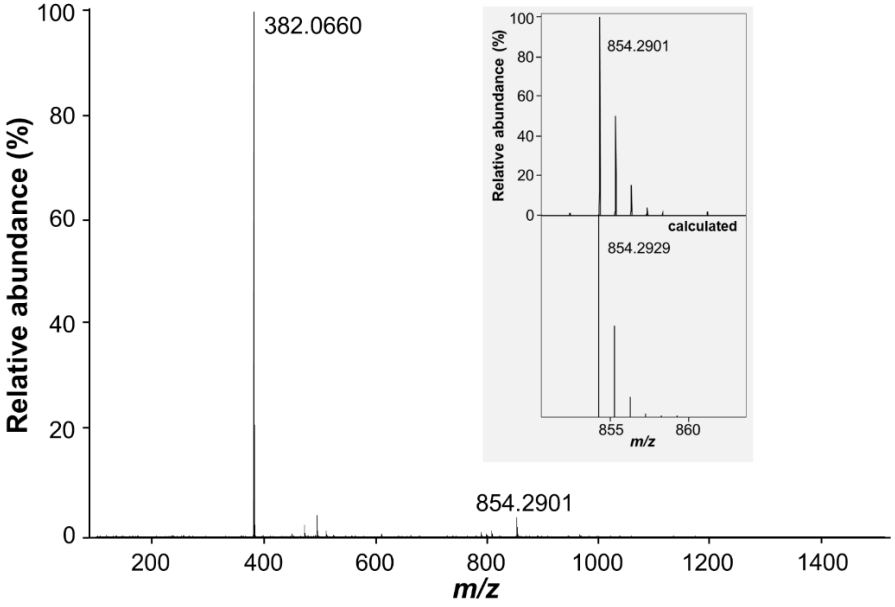

Figure S22. ESI-mass spectrum of **1c**. The inset shows the peak at *m/z* 854.2901 assigned to [**1c** – PF_6]$^+$ (m/z_{calc} 854.2929).

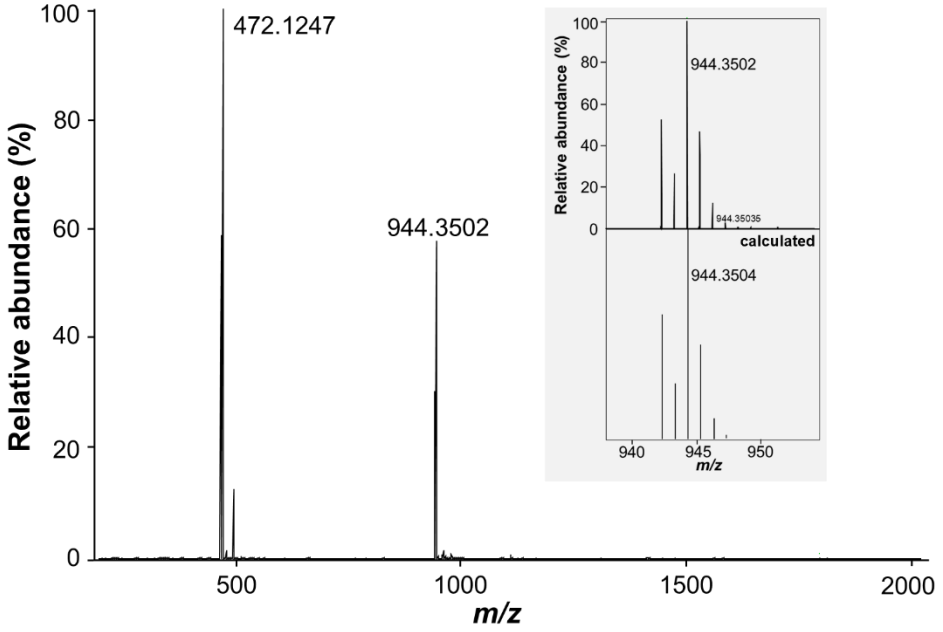

Figure S23. ESI-mass spectrum of **1d**. The inset shows the peak at *m/z* 944.3502 assigned to [**1d** – PF_6]$^+$ (m/z_{calc} 944.3504).

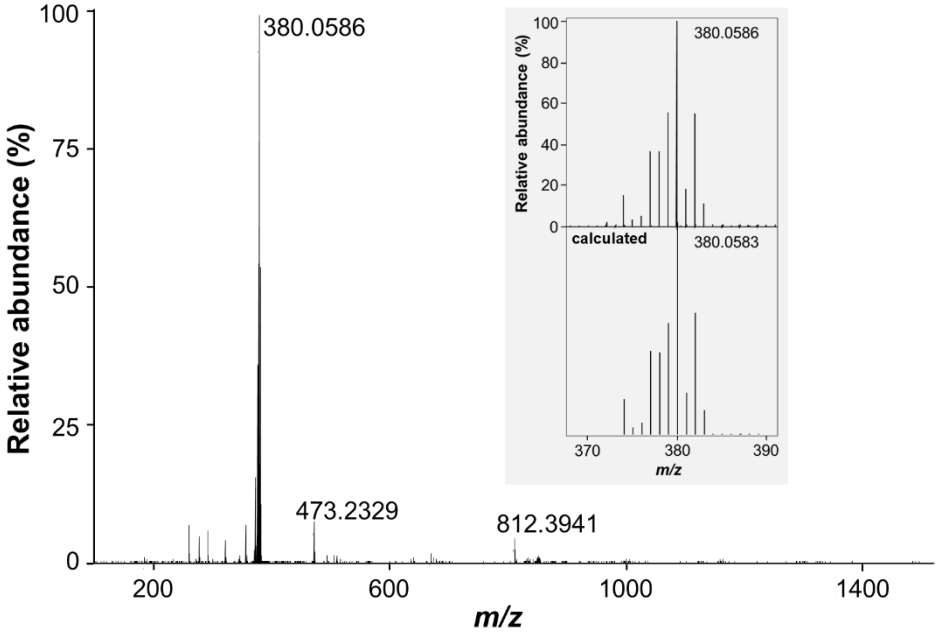

Figure S24. ESI-mass spectrum of **2a**. The inset shows the peak at *m/z* 380.0586 assigned to [**2a** – PF_6 – **L2**]$^+$ (m/z_{calc} 380.0583).

Zebrafish embryo toxicity data

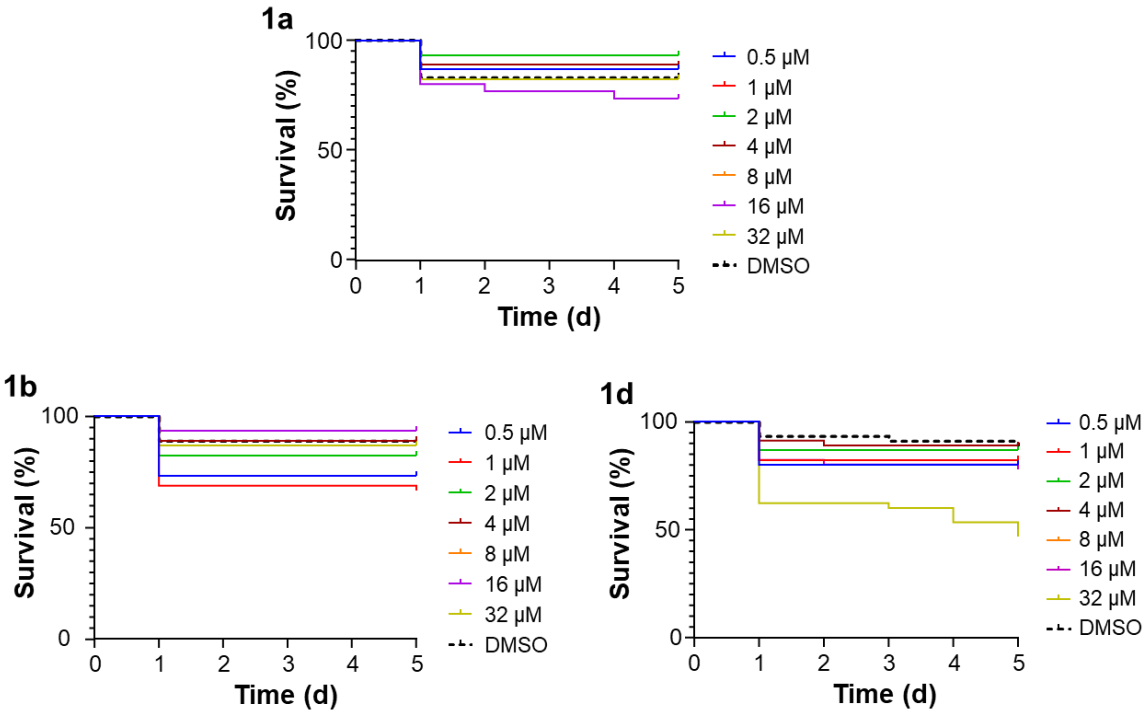

Figure S25. Kaplan Meier plot tracking the survival of zebrafish embryos treated over three replicate experiments with **1a**, **1b** and **1d** over 5 d at concentrations ranging from 0.5 to 32 µM.

UV-Vis and ESI-mass spectra for biomolecule binding assays

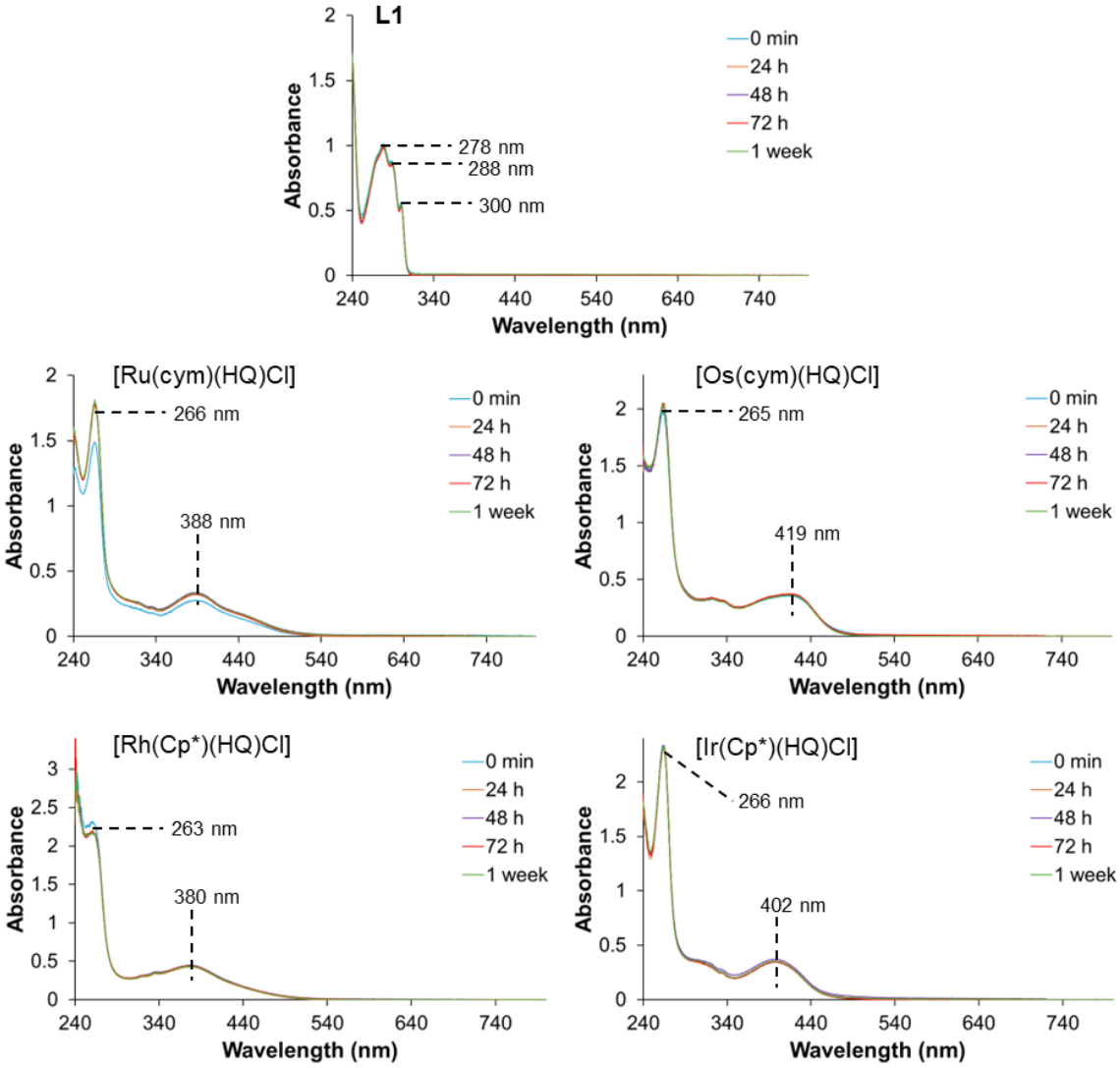

Figure S26. Stability study of AmInd-BAHA ligand **L1** and non-biotinylated parent complexes [M(cym/Cp*)(HQ)Cl] in 10% DMSO/H_2O by UV-Vis absorption spectroscopy over the course of 1 week.

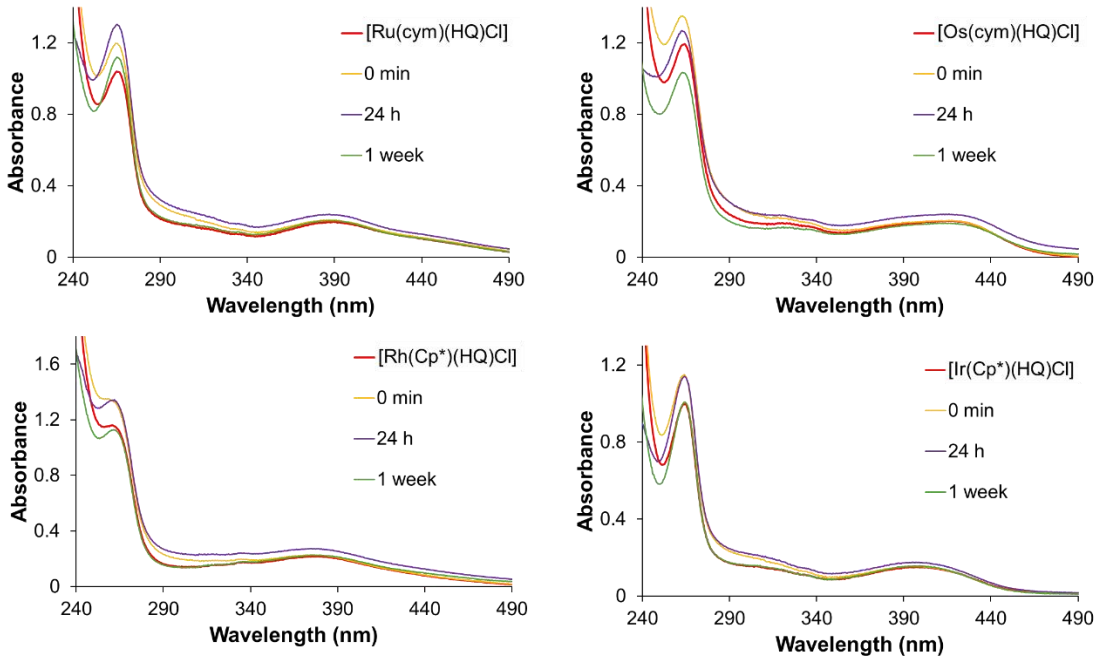

Figure S27. UV-Vis spectra of non-biotinylated [M(cym/Cp*)(HQ)Cl] complexes (red lines) in 10% DMSO/H_2O as well as those with the addition of 2 equiv. $AgNO_3$ over the course of 1 week.

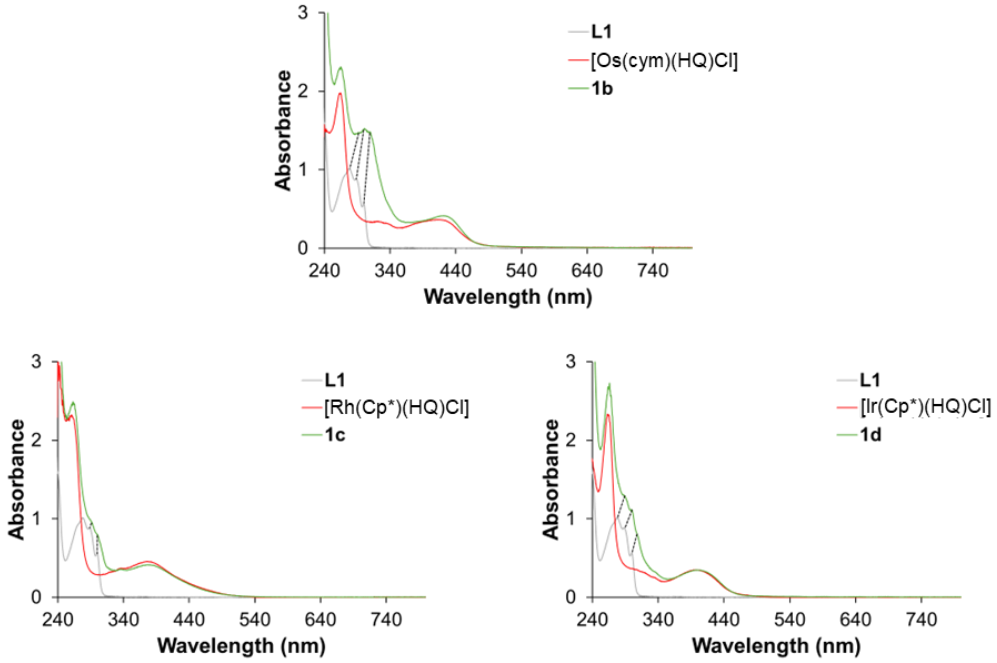

Figure S28. Comparative UV-Vis absorption spectra of biotinylated HQ complexes **1b**–**1d** against biotinyl-aminoindazole ligand **L1** and their respective non-biotinylated chlorido complexes.

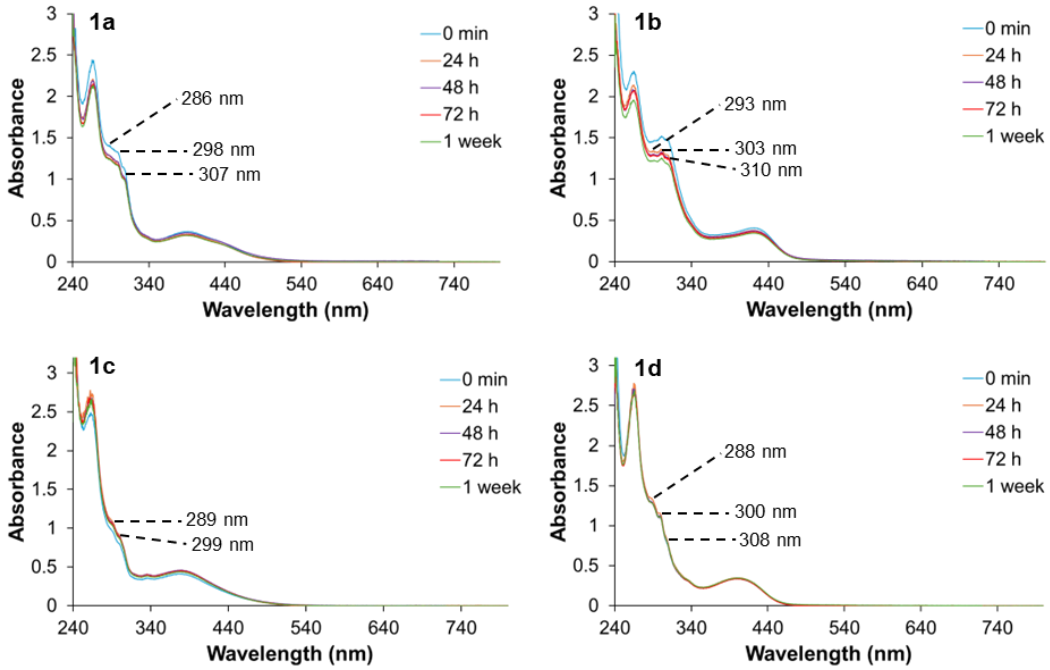

Figure S29. Stability study of biotinylated complexes **1a**–**1d** in 10% DMSO/H_2O by UV-Vis over the course of 1 week.

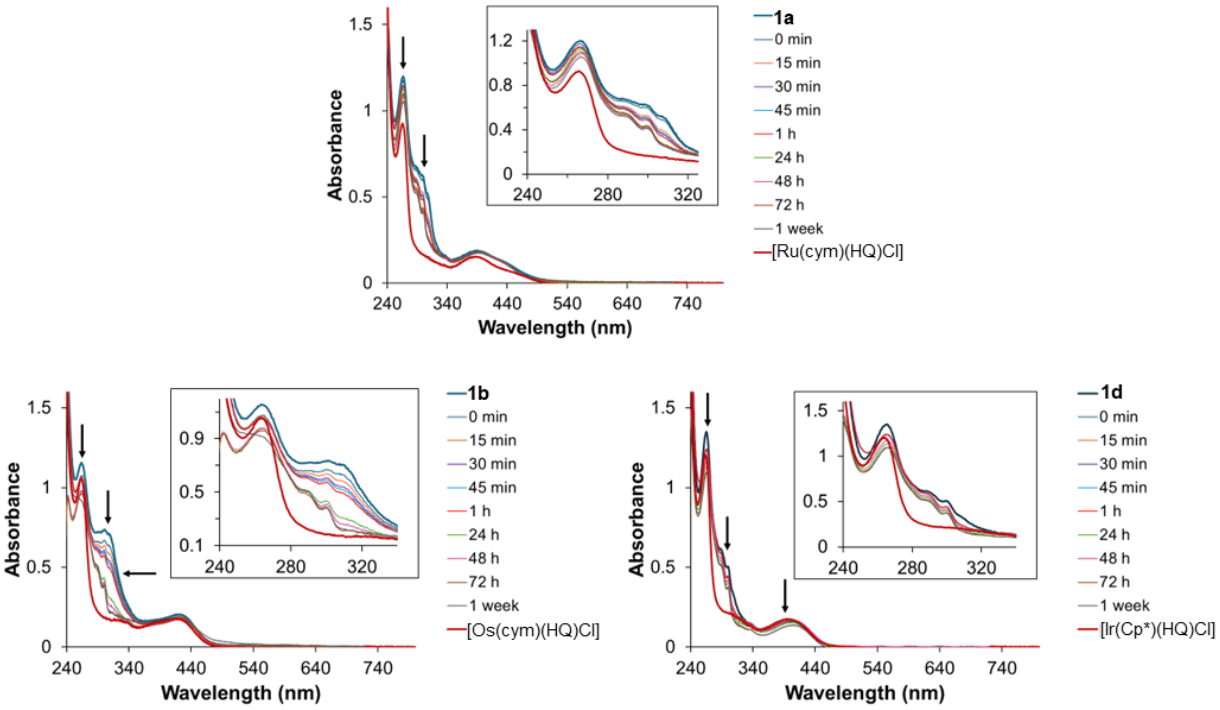

Figure S30. UV-Vis absorption spectra of complexes **1a**, **1b** and **1d** in 10% DMSO/H_2O before incubation with L-histidine as well as at several time intervals after incubation, including spectra of their respective non biotinylated [M(cym/Cp*)(HQ)Cl] complexes.

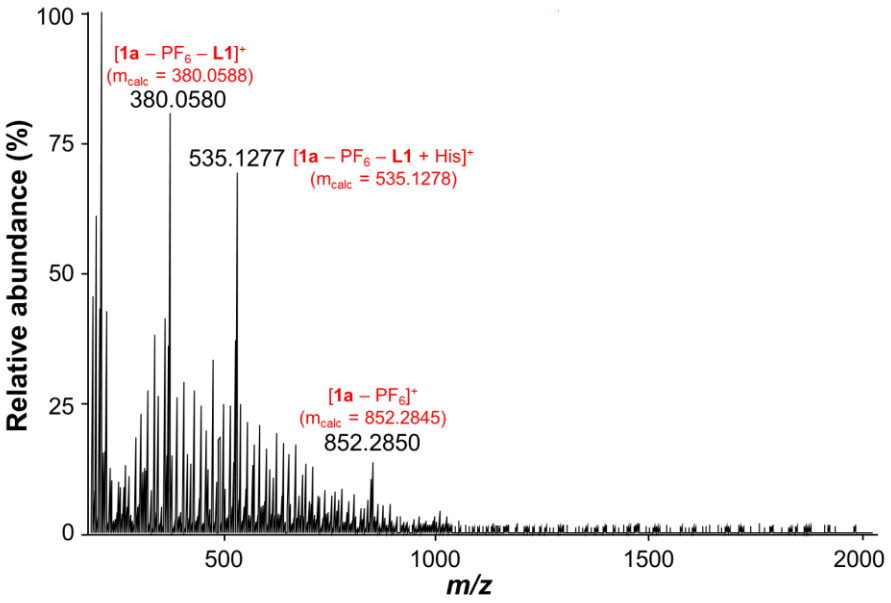

Figure S31. ESI-mass spectrum of **1a** incubated with L-histidine (His) for 1 week indicating relevant peaks.

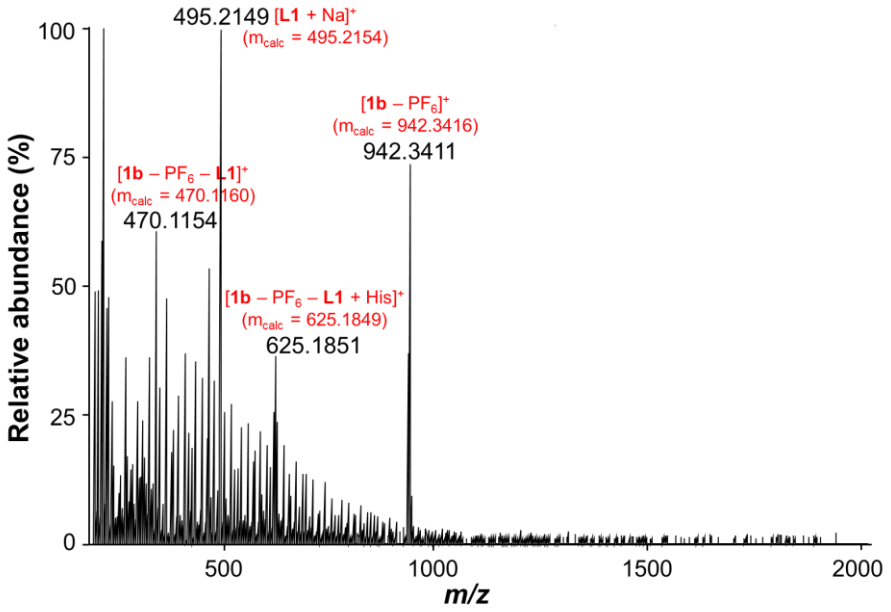

Figure S32. ESI-mass spectrum of **1b** incubated with L-histidine (His) for 1 week indicating relevant peaks.

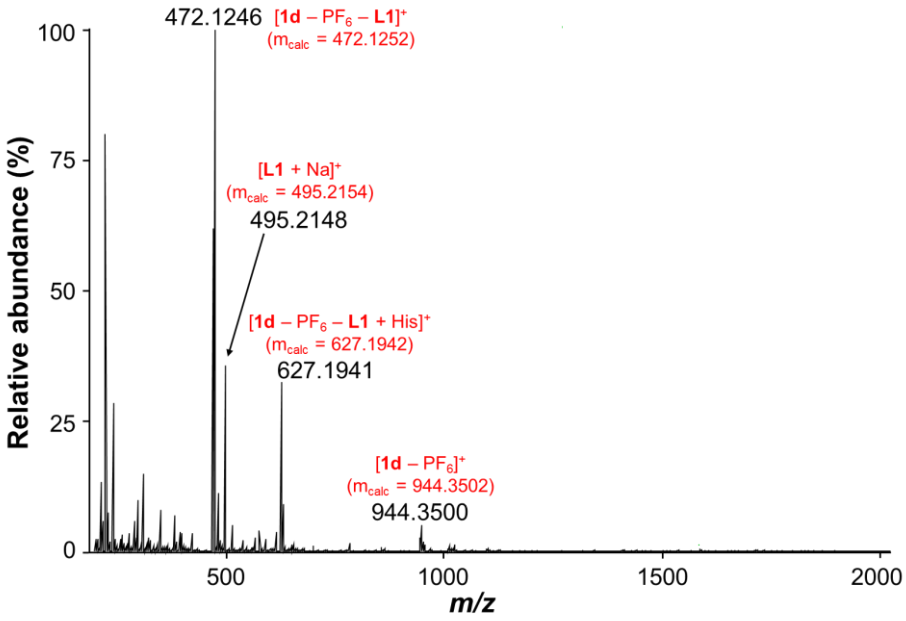

Figure S33. ESI-mass spectrum of **1d** incubated with L-histidine (His) for 1 week indicating relevant peaks.

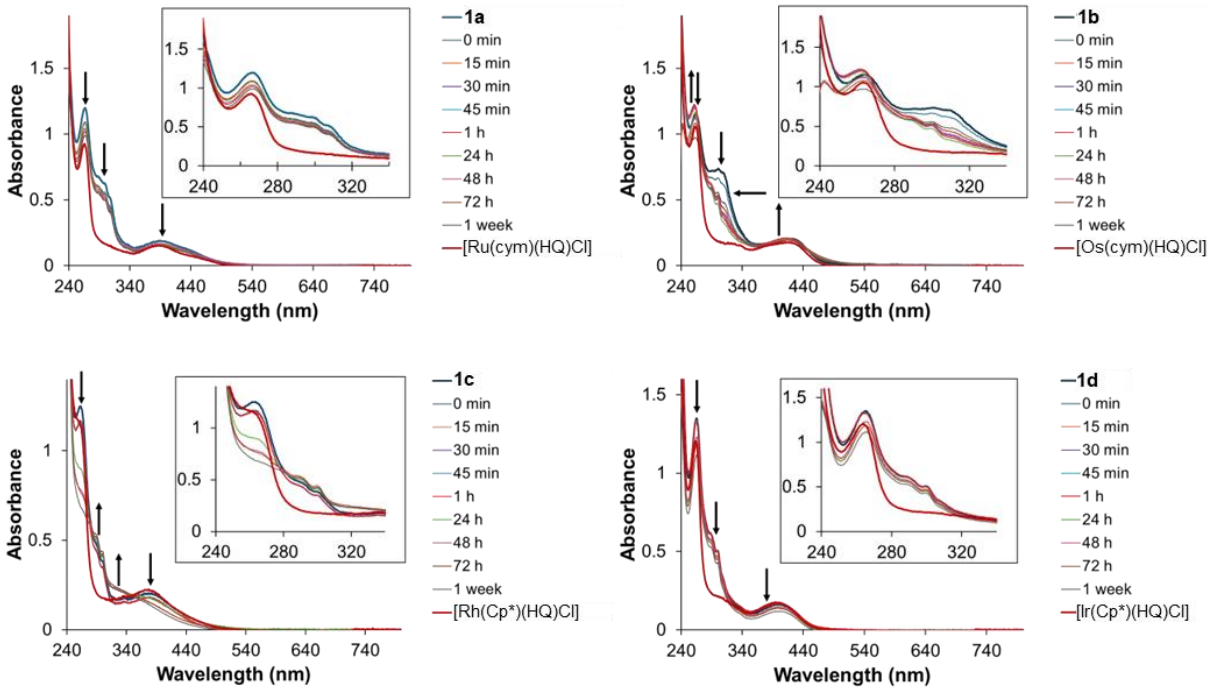

Figure S34. UV-Vis absorption spectra of complexes **1a**–**1d** in 10% DMSO/H_2O before incubation with L-cysteine as well as at several time intervals after incubation, including spectra of their respective non biotinylated [M(cym/Cp*)(HQ)Cl] complexes.

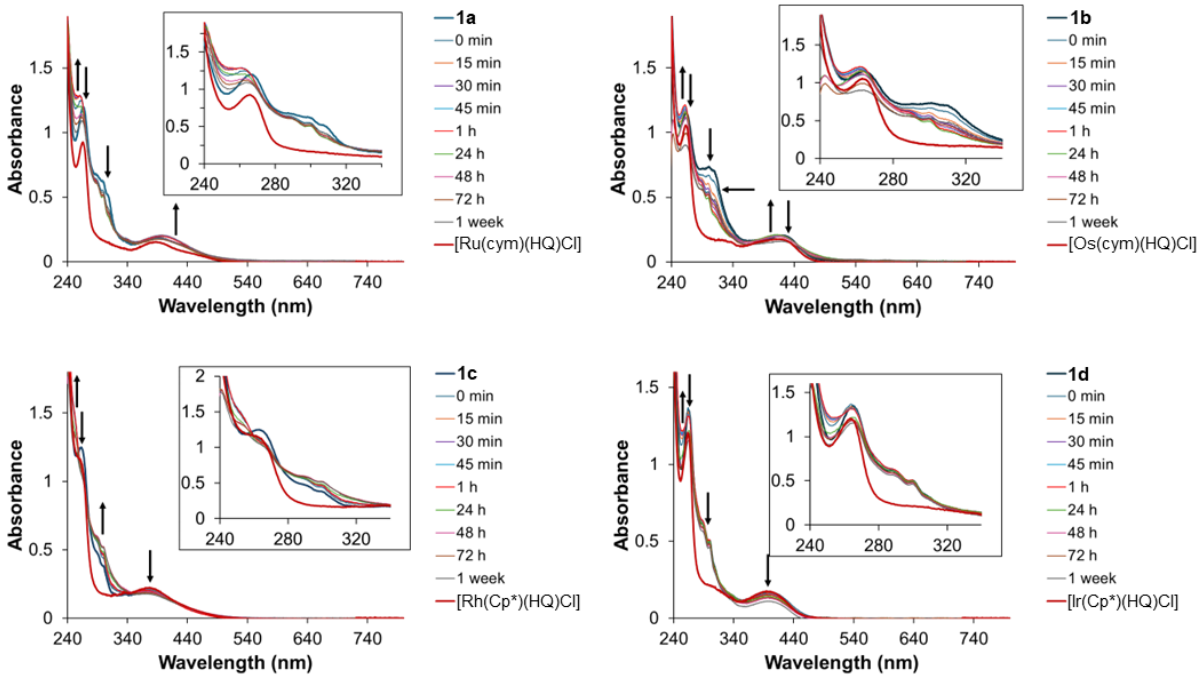

Figure S35. UV-Vis absorption spectra of complexes **1a**–**1d** in 10% DMSO/H_2O before incubation with glutathione as well as at several time intervals after incubation, including spectra of their respective non biotinylated [M(cym/Cp*)(HQ)Cl] complexes.

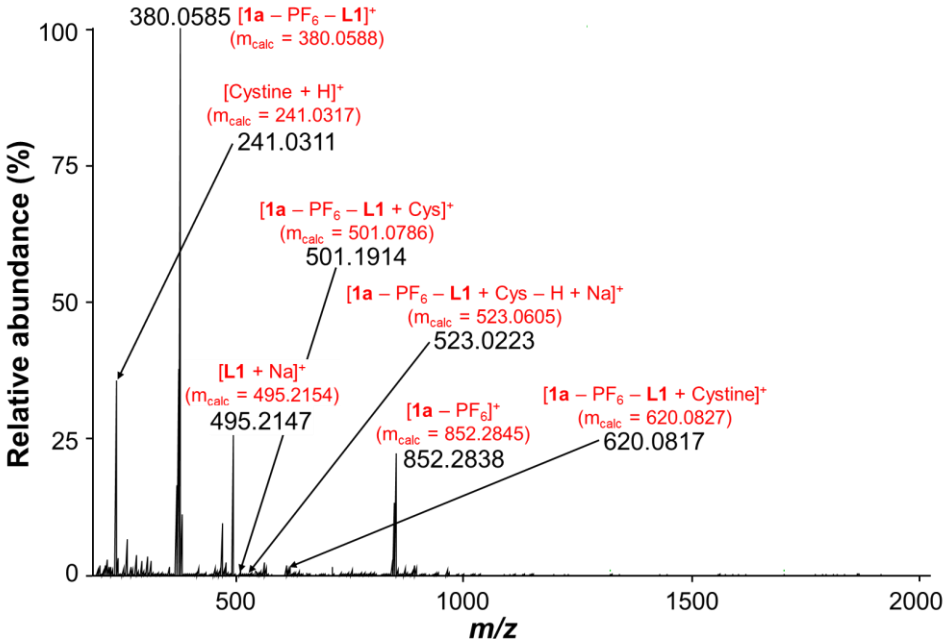

Figure S36. ESI-mass spectrum of **1a** incubated with L-cysteine (Cys) for 1 week indicating relevant peaks.

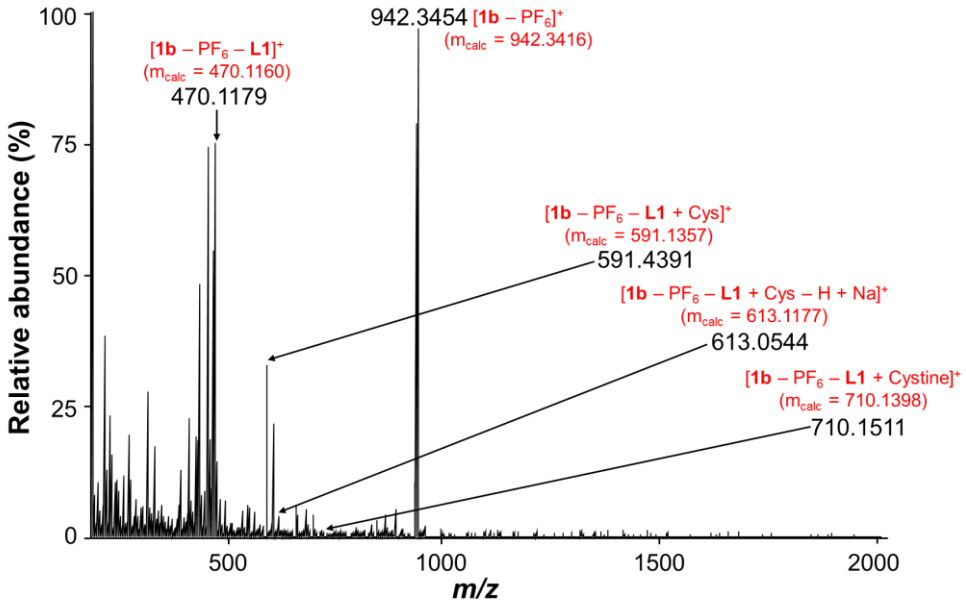

Figure S37. ESI-mass spectrum of **1b** incubated with L-cysteine (Cys) for 1 week indicating relevant peaks.

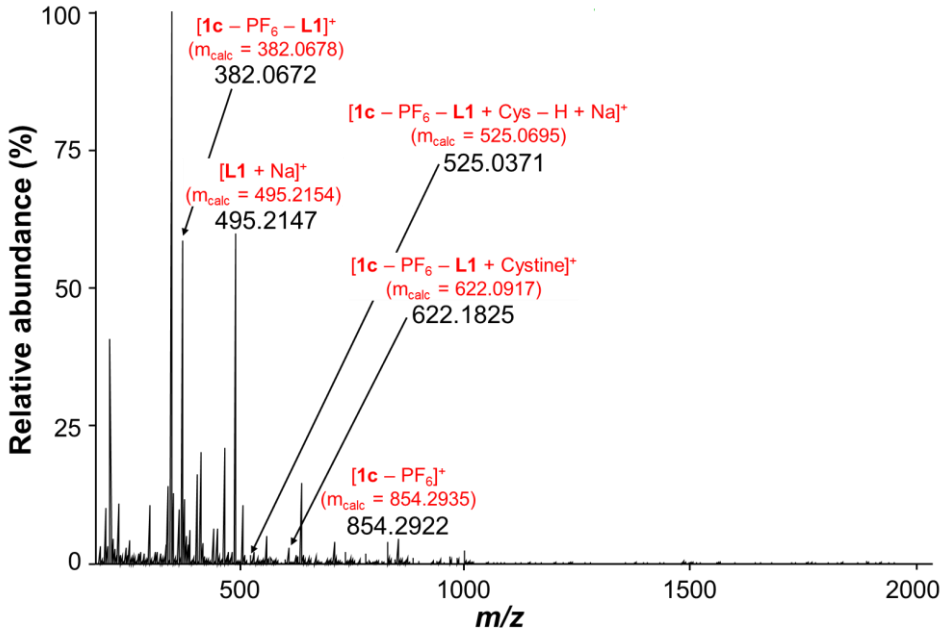

Figure S38. ESI-mass spectrum of **1c** incubated with L-cysteine (Cys) for 1 week indicating relevant peaks.

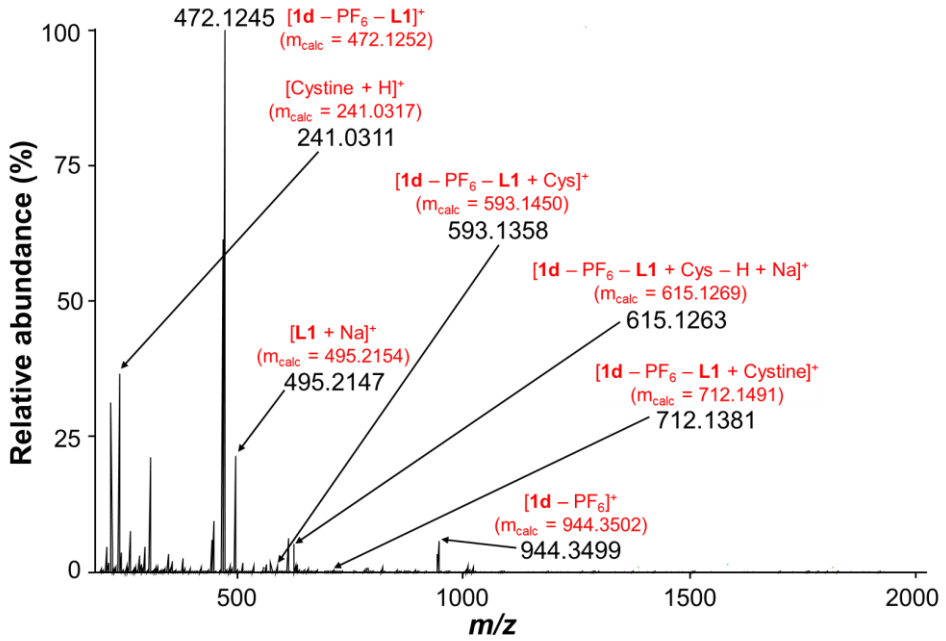

Figure S39. ESI-mass spectrum of **1d** incubated with L-cysteine (Cys) for 1 week indicating relevant peaks.

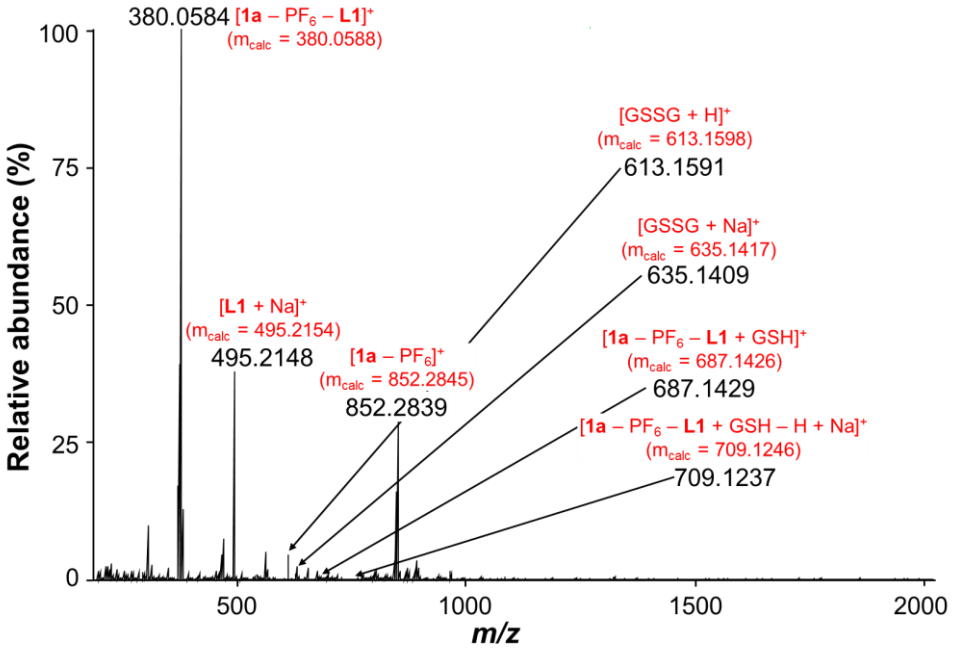

Figure S40. ESI-mass spectrum of **1a** incubated with glutathione (GSH) for 1 week indicating relevant peaks.

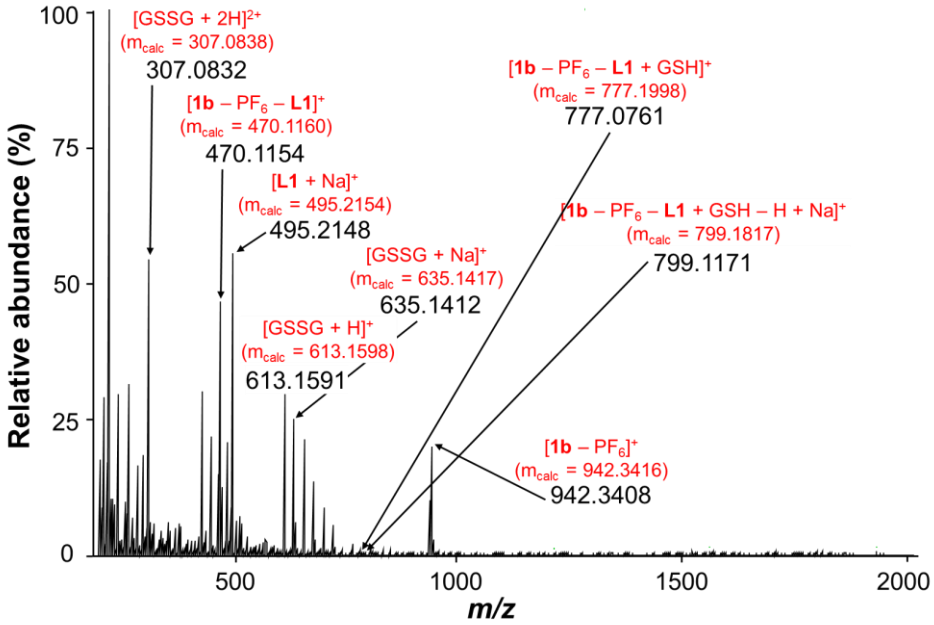

Figure S41. ESI-mass spectrum of **1b** incubated with glutathione (GSH) for 1 week indicating relevant peaks.

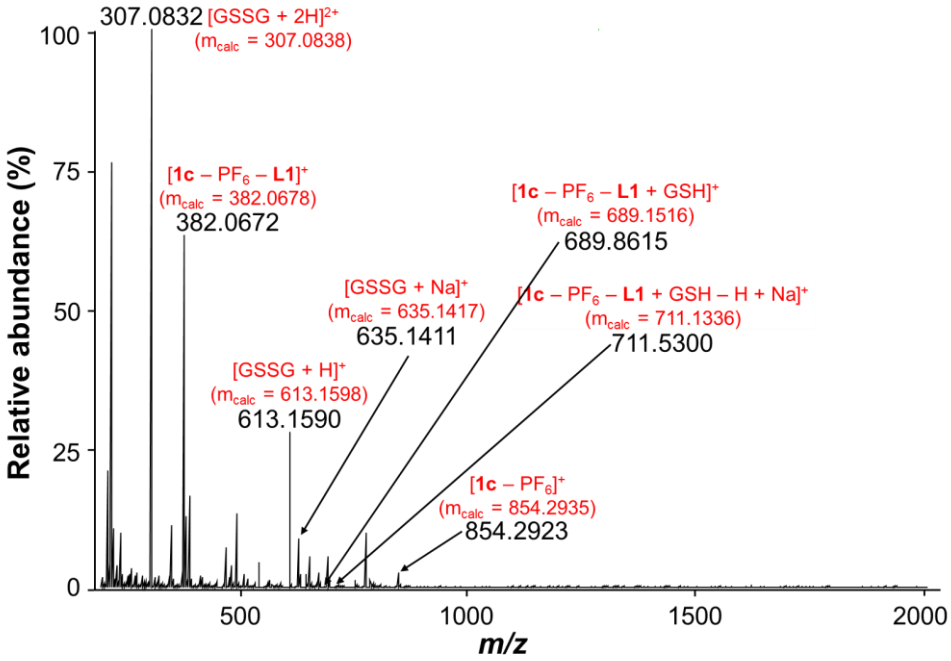

Figure S42. ESI-mass spectrum of **1c** incubated with glutathione (GSH) for 1 week indicating relevant peaks.

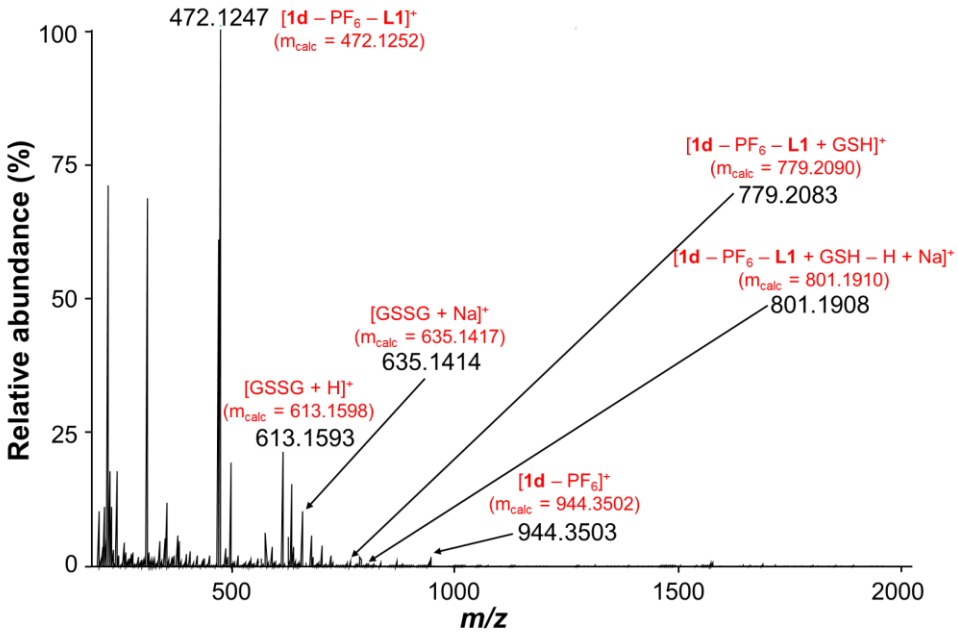

Figure S43. ESI-mass spectrum of **1d** incubated with glutathione (GSH) for 1 week indicating relevant peaks.

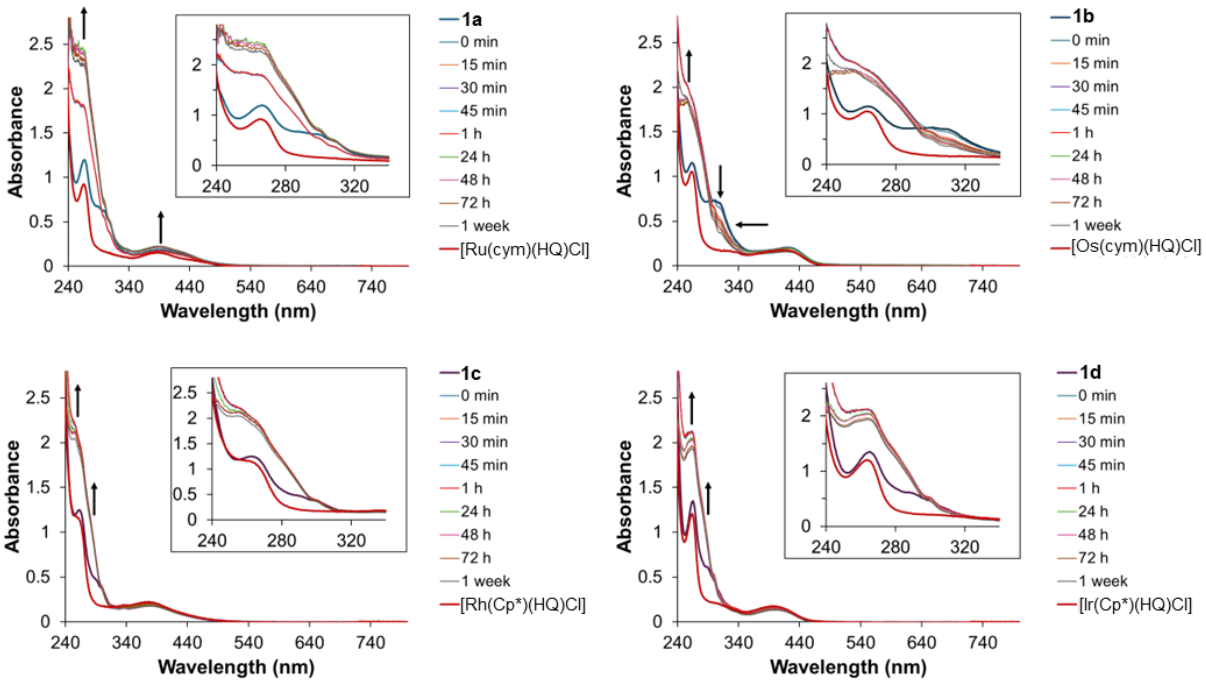

S44. UV-Vis absorption spectra of complexes **1a**–**1d** in 10% DMSO/H_2O before incubation with 9-ethylguanine (9EtG) as well as at several time intervals after incubation, including spectra of their respective non biotinylated [M(cym/Cp*)(HQ)Cl] complexes.

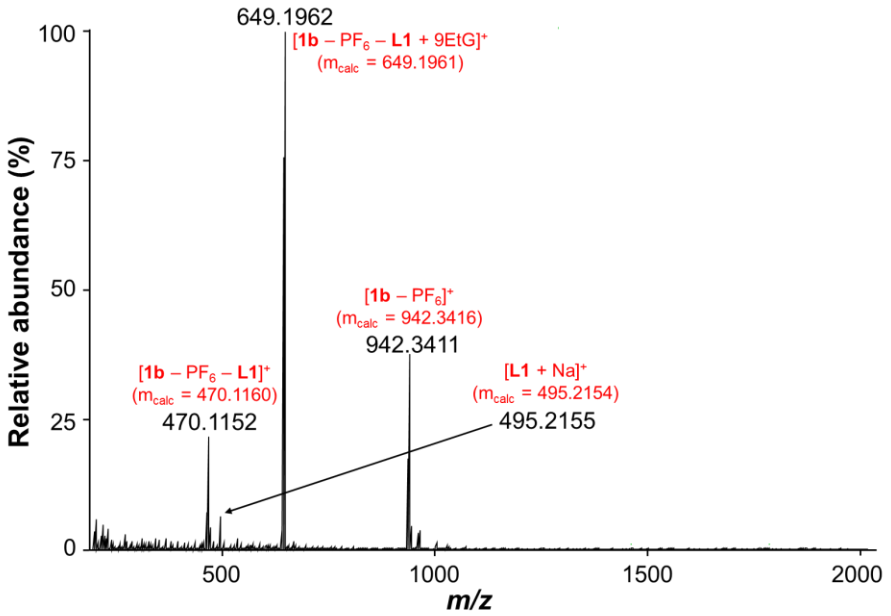

Figure S45. ESI-mass spectrum of **1b** incubated with 9-ethylguanine (9EtG) for 1 week indicating relevant peaks.

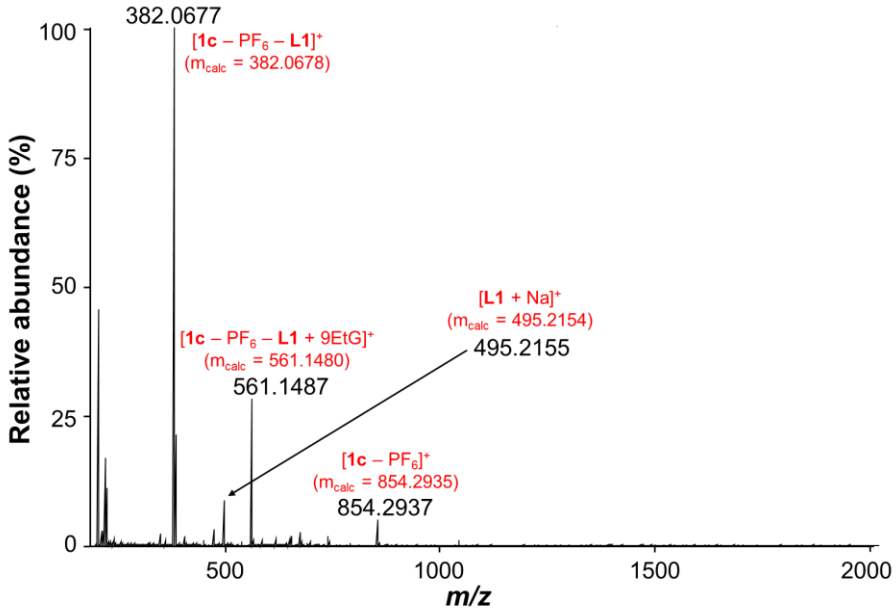

Figure S46. ESI-mass spectrum of **1c** incubated with 9-ethylguanine (9EtG) for 1 week indicating relevant peaks.

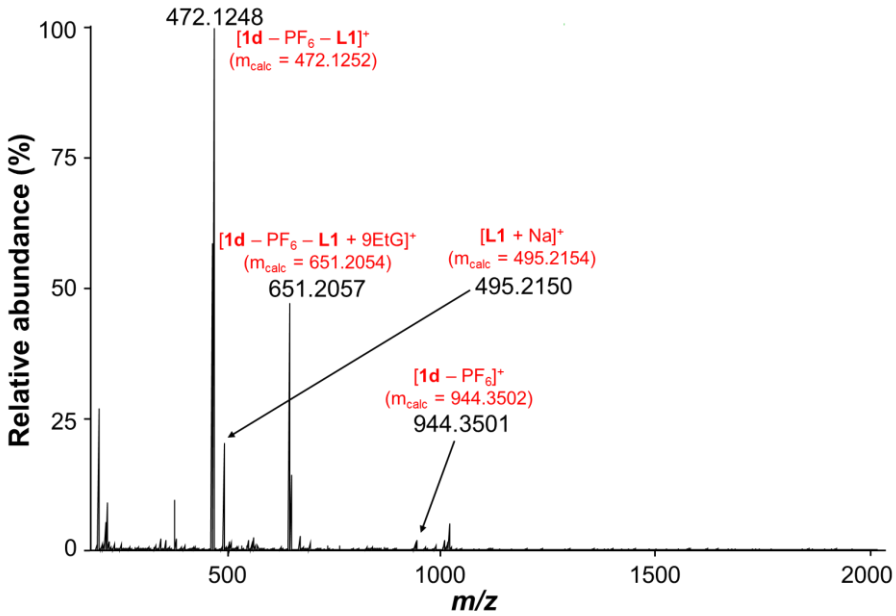

Figure S47. ESI-mass spectrum of **1d** incubated with 9-ethylguanine (9EtG) for 1 week indicating relevant peaks.

Table S1. GoldScore docking scores for both enantiomers of compounds **1a**–**1d** with regard to the configuration at the metal center (**1a**-M_R, **1a**-M_S, **1b**-M_R, **1b**-M_S, **1c**-M_R, **1c**-M_S, **1d**-M_R, **1d**-M_S) at the biotin binding site of streptavidin (PDB ID: 3YR2), as predicted by GOLD, including root mean square deviation (RMSD) values relative to the positioning of co-crystallized biotin.

Compound	GoldScore	RMSD (Å)
Biotin	73.8	0.21
1a-M_S	88.7	0.64
1a-M_R	91.7	0.44
1b-M_S	102	0.70
1b-M_R	92.7	0.33
1c-M_S	88.2	0.78
1c-M_R	85.8	0.68
1d-M_S	102	0.70
1d-M_R	95.3	0.75

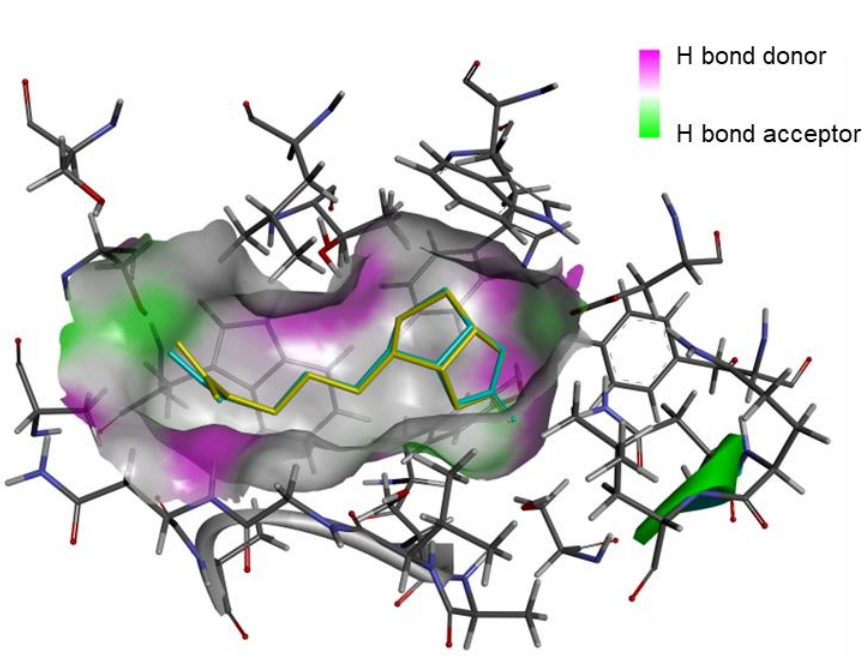

Figure S48. The minimum energy docked pose of biotin with streptavidin (PDB ID: 3YR2) indicating hydrogen bonding interactions, as predicted by GOLD.

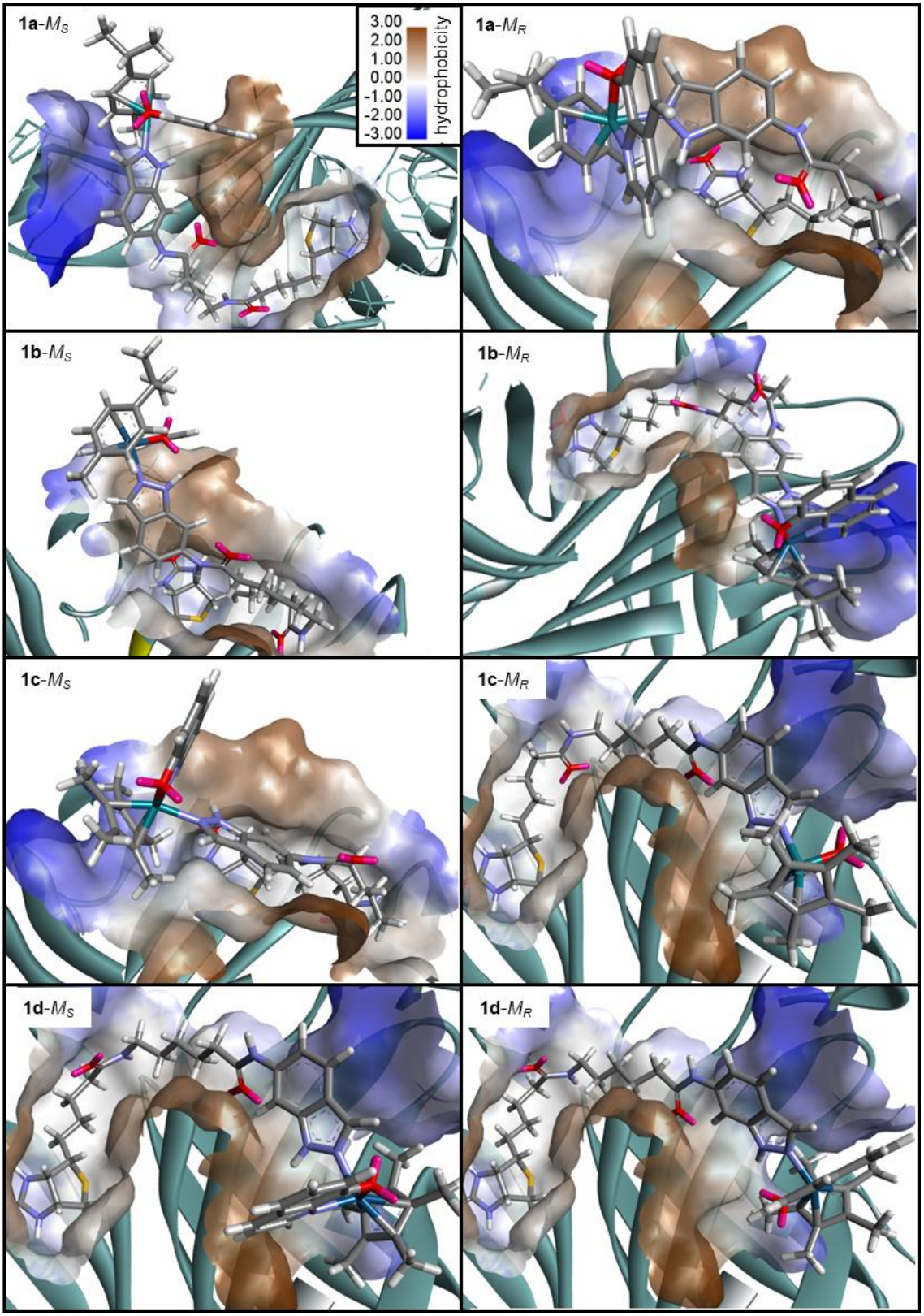

Figure S49. The highest scoring poses of both enantiomers of compounds **1a**–**1d** with regard to the configuration at the metal center (**1a**-M_R, **1a**-M_S, **1b**-M_R, **1b**-M_S, **1c**-M_R, **1c**-M_S, **1d**-M_R, **1d**-M_S) in docking studies at the biotin binding site of streptavidin (PDB ID: 3YR2), as predicted by GOLD. The protein surface is rendered to depict hydrophilic regions on the surface in blue, hydrophobic regions in brown, and neutral areas in grey.